On the Performance of NOMA-enabled Multi-Sector RIS-aided with ISAC

Abhinav Singh Parihar*, Keshav Singh*, Chih-Peng Li*, Vimal Bhatia+†, and Trung Q. Duong§
*Institute of Communications Engineering, National Sun Yat-sen University, Kaohsiung 80424, Taiwan
+Department of Electrical Engineering, Indian Institute of Technology Indore, Indore, India
†School of Electronic and Information Engineering, Soochow University, Suzhou 215006, China
§Faculty of Engineering and Applied Science, Memorial University, NL A1C 5S7, Canada
E-mail: abhinavsingh2304@gmail.com, keshav.singh@mail.nsysu.edu.tw, cpli@faculty.nsysu.edu.tw, vbhatia@iiti.ac.in, tduong@mun.ca

***Abstract*—With the arrival of sixth-generation communication systems, advanced technologies like multi-input single-output (MISO), reconfigurable intelligent surfaces (RIS), and integrated sensing and communication (ISAC) are poised to drive a broad range of Internet of Things (IoT) applications. Integrating ISAC into MISO networks, however, calls for a reassessment of performance metrics such as outage probability and sensing rate. In this work, we propose an innovative multi-sector RIS framework that partitions the surface into independently controlled sectors, each dynamically selecting the closest sector to target users, who are assumed to be distributed following a Poisson point process (PPP). For downlink transmissions, this multi-sector RIS design combines phase-shift control and simultaneous transmission/reflection within the chosen sector. Our approach includes a nearest-sector selection strategy around a reference user, with closed-form approximations for the outage probability derived under the assumption of a blocked direct link between the base station (BS) and users. The framework also enables ISAC by transmitting sensing signals within the selected sector, facilitating both user communication and target detection. Sensing performance is characterized by the sensing rate, with results showing that increasing RIS elements in the multi-sector design significantly enhances sensing capabilities. Overall, the proposed system demonstrates superior performance over traditional STAR-RIS configurations.**

***Index Terms*—Integrated sensing and communication (ISAC), multi-input single-output (MISO), multi-sector, Poisson point process (PPP), reconfigurable intelligent surfaces (RIS).**

I. Introduction

The Internet of Things (IoT) envisions a future where devices communicate autonomously, without human intervention [1], thereby enabling a wide range of applications—from smart cities and connected vehicles to healthcare and more. Cellular networks are ideally positioned to support IoT communications, providing a robust foundation for various IoT services. To meet the escalating demand and the growing traffic generated by IoT, 6G network architectures are integrating multiple-input single-output (MISO) technologies [2]. Given the unprecedented sensing requirements of upcoming wireless networks, there is a strong push towards integrating radio sensing within communication systems. A key design challenge in integrated sensing and communication (ISAC) is to identify efficient and cost-effective solutions that align with existing network architectures [3]. While communication utilizes radio waves to relay signals between a transmitter and a receiver, sensing relies on analyzing radio frequency echoes reflected from a target. By processing these echoes, target parameters such as location, velocity, and dimensions can be determined, often through conventional or learning-based techniques [4]. One feasible approach is to introduce minimal modifications to current communication models, enabling them to also support sensing functions [5].

Reconfigurable intelligent surface (RIS)-enabled wireless communications have attracted significant attention, as demonstrated in studies such as [6]–[9], for enhanced coverage. For instance, [10] examined a full-duplex system with Nakagami-m fading, where a full-duplex transceiver facilitated downlink and through two RISs, each operating in full-duplex mode. In [11], the outage probability (OP) and symbol error rate (SER) were derived for RIS-assisted wireless communications over Rayleigh fading channels. Performance evaluation under Nakagami-m fading, specifically the coverage probability, was conducted in [12] by leveraging moment-generating functions for RIS-enabled systems. The impact of the line-of-sight (LoS) link was further analyzed in [13], which evaluated the OP, ergodic rate, and average SER for RIS-based networks under Rician fading. Additionally, [14] addressed the resource allocation problem for spectrally efficient full-duplex RIS systems. [15] developed a system model for active STAR-RISs, focusing on the analysis of their communication performance enhancements. [16] explored the integration of STAR-RIS with NOMA systems, focusing on optimizing location and beamforming to improve system efficiency. [17] delved into the use of non-diagonal phase shift matrices in RIS, presenting new possibilities for system design. [18] investigated strategies for the deployment and beamforming of STAR-RIS to optimize communication performance. [19] examined the interplay between transmitting waveform design and passive beamforming in RIS-aided ISAC systems, providing a novel approach to enhance sensing and communication.

A. Motivation and contribution

The RIS structures described in [6]–[8], [10]–[14], [20], have limited applications, assumed that the incident signal could

only be reflected from the same place after modification. Put simply, there was no connection between the elements of the RIS, such RIS are termed the conventional RIS. Consequently, the phase shift matrix exhibited a diagonal structure, failing to leverage RIS's potential to enhance system performance fully. Conversely, a new multi-sector RIS configuration is introduced, which enables the transmission of incident signals from one sector to another through precise phase shift calibration. Furthermore, most of the current works assumed the BS to have a single antenna, hence the integration of MISO technology in ISAC networks has not been extensively studied. This work aims also to fill this gap. The primary contributions are:

- A multi-sector RIS is considered by partitioning the surface into sectors, each of which can independently control its phase shifts and reflections/refracting behaviour to target different users. The uses are homogeneous Poisson point process (PPP) distributed, and the RIS dynamically selects the sector closest to the user based on location.
- The nearest sector selection strategy is applied, centred around a reference user at the origin and approximate closed-form expressions for the OP are derived, assuming a blocked direct link between the base station (BS) and the user.
- To support ISAC, the BS also transmits a sensing signal within the selected sector for target detection. Thus, each sector not only relays communication signals to users but also facilitates target sensing, integrating the two functions within the same RIS-assisted framework.
- The sensing performance of multi-sector RIS is characterized by calculating the sensing rate. It is shown that increasing the RIS elements can enhance the sensing rate in the multi-sector RIS.

B. Paper organization

Section II presents the system model. Section III focuses on deriving analytical expressions for OP. In Section IV, both analytical and simulation results are examined. Finally, Section V provides the conclusions.

Notation: Lower and uppercase bold letters denote vectors and matrices, respectively. The conjugate transpose of a matrix or vector is indicated by $(\cdot)^H$. The notations $\|\cdot\|$ and $|\cdot|$ stand for the Euclidean norm and the modulus operation, respectively. For any matrix $\mathbf{C}$, $\mathrm{Tr}(\mathbf{C})$ refers to its trace, and $\mathrm{diag}(\mathbf{C})$ extracts its diagonal elements as a vector. The notation $\mathcal{CN}(0,\sigma^2)$ describes a complex Gaussian random variable with zero mean and variance σ^2. Complex matrices of size $P \times Q$ are represented by $\mathbb{C}^{P\times Q}$. The notation $\mathbb{E}[\cdot]$ represents the expectation operator. The identity matrix of order M is written as $\mathbf{I}_M$. Lastly, $\mathrm{P}[\mathcal{A}]$ designates the probability of event $\mathcal{A}$ occurring.

II. System Model

We consider a multi-sector RIS-assisted ISAC system as depicted in Fig. 1. The BS is equipped with M_t transmit

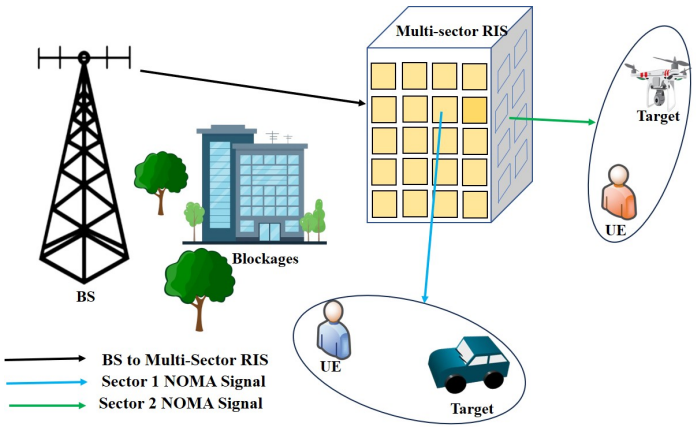

Fig. 1: Overview of the proposed system model.

antenna and M_r receive antenna, allowing it to serve users and simultaneously receive signals for target detection. For simplicity, it is assumed that $M_r = M_t$. The multi-sector RIS contains N sectors each having R elements. Therefore the coverage area is divided into N sections based upon the number of sectors. The users are distributed as a homogeneous PPP denoted as Ω_u with density λ_u. It is assumed that a direct connection between the BS and users is blocked. The users are served by the help of multi-sector RIS which provides full space coverage. The users are selected based on the nearest sector selection scheme wherein the sector closest to the user is assigned. NOMA is used by the BS to serve the user and also transmit a sensing signal on the selected section of the sector to sense the presence of the target. To carry out the transmission, the BS simultaneously sends the dedicated sensing signals x_t and the communication symbol x_k for the k-th user. Specifically, considering that the $x_k \sim \mathcal{CN}(0,1)$ and $x_t \sim \mathcal{CN}(0,\mathbf{R}_t)$, where $\mathbf{R}_t = \mathbb{E}[\mathbf{x}_t\mathbf{x}_t^H]$, and $\{\mathbf{x}_k, \mathbf{x}_t\}$ are statistically independent. Thus, the joint signal sent by the BS is given by

$$\mathbf{x} = \sum_{k=1}^{K} \mathbf{w}_k \mathbf{x}_k + \mathbf{x}_t, \tag{1}$$

where the beamforming vector for symbol $\mathbf{x}_k$ is represented by $\mathbf{w}_k$. From (1), the transmitted power is evaluated as $\mathbb{E}[\|\mathbf{x}\|^2] = \sum_{k=1}^{K} \|\mathbf{w}_k\|^2 + \mathrm{Tr}(\mathbf{R}_t)$. Furthermore, the sensing signal x_t is the general multi-beam transmit signal [21]. Consequently, employing the eigenvalue decomposition (EVD) of $\mathbf{R}_t$, $\mathbf{x}_t$ is further written as

$$\mathbf{x}_t = \sum_{i=1}^{\mathrm{rank}(\mathbf{R}_t)} \mathbf{w}_{t,i} x_{t,i}, \tag{2}$$

where all sensing waveforms follow $\mathcal{CN}(0,1)$, and $\mathbf{w}_{t,i}$ denotes the beamformer.

A. Multi-sector RIS Model

The RIS elements across all sectors are connected by reconfigurable impedances and thus support the multi-sector

transmission. The sector n serves $1/N$ of the coverage area which belongs to $\mathcal{R}_n = \{(n-1)R+1, \ldots, nR\}, \forall n \in \mathcal{N} = \{1, \ldots, N\}$. The BS is connected to the sector 1. Moreover, the BS is out of coverage for the sector n, such that $\forall n \in N, n \neq 1$. Therefore, the multi-sector-RIS utilizes the energy splitting (ES) protocol. Each sector elements transmits the signal, directing them into N separate spaces, enabling sensing and communication in all directions. We denote $\mathbf{\Psi}_n \in \mathbb{C}^{R\times R}$ as the phase shift matrices for the transmission from n-th sector, which is mathematically modelled as

$$\mathbf{\Psi}_n = \text{diag}\left(\sqrt{\Lambda_{(n-1)R+1}}e^{\psi_{(n-1)R+1}}, \ldots, \sqrt{\Lambda_{nR}}e^{\psi_{nR}}\right), \tag{3}$$

where $\sqrt{\Lambda_i} \in [0,1]$ and $\psi_i \in [0, 2\pi)$ are the amplitude and phase-shift of the n-th sector's r-th element transmission coefficient. The phase shift matrix satisfies the constraint represented as

$$\sum_n \mathbf{\Psi}_n^H \mathbf{\Psi}_n = \mathbf{I}_R \tag{4}$$

B. Channel Model

In this model, we assume a LoS link between the BS and sector 1 of the RIS because the BS and RIS are in sector 1. Nakagami-m fading characterizes the BS-to-RIS and RIS-to-user links. The channel between the BS and sector 1 of the RIS, $\mathbf{H}_1$, is modelled as an $R \times M_t$ matrix with Nakagami-m fading parameter m_1. This matrix captures the gain between the t-th transmit antenna at the BS and the r-th element within sector 1 of the RIS, expressed as:

$$\mathbf{H}_1 = \begin{bmatrix} h_{1,1} & \cdots & h_{1,M_t} \\ \vdots & \ldots & \vdots \\ h_{R,1} & \cdots & h_{R,M_t} \end{bmatrix}, \tag{5}$$

where each entry $h_{r,m} \sim$ Nakagami$(m_1, 1)$ represents the channel gain from the m-th BS antenna to the r-th element in sector 1 of the RIS. The users, modeled by a PPP distribution, are located within the coverage area of the multi-sector RIS. Each user connects to the RIS through the closest sector based on proximity, ensuring optimal signal strength. The channel from the selected RIS sector to the user UE$_k$ is denoted by $\mathbf{g}_k$, a $1 \times R$ vector also following Nakagami-m fading with parameter m_2. For a selected RIS sector n closest to user UE$_k$, the channel matrix is represented as:

$$\mathbf{g}_k = \begin{bmatrix} g_{k,1} & \cdots & g_{k,R} \end{bmatrix}, \tag{6}$$

where each $g_{k,r} \sim$ Nakagami$(m_2, 1)$ models the fading between the r-th element of sector n and the receiving antenna of UE$_k$. Each sector, $\mathbf{\Psi}_n$, is configured with a phase shift matrix to optimize signal reflection and transmission toward its users. This multi-sector approach enables each RIS sector to operate independently, directing energy to both support communication and conduct sensing for users within its designated area.

C. Communication SINR

The signal that was received by the k-th user from the multi-sector RIS is expressed as

$$\begin{aligned} y_k =& \mathbf{g}_k \mathbf{\Psi}_f \mathbf{H}_k \mathbf{w}_k x_k + \underbrace{\sum\nolimits_{i\neq k} \mathbf{g}_k \mathbf{\Psi}_f \mathbf{H}_k \mathbf{w}_i \mathbf{x}_i}_{\text{inter user interference}} \\ &+ \underbrace{\mathbf{g}_k \mathbf{\Psi}_f \mathbf{H}_k \mathbf{x}_t}_{\text{sensing interference}} + n_k, \end{aligned} \tag{7}$$

where $n_k \sim \mathcal{CN}(0, \sigma_k^2)$ is AWGN noise at the k-th user.

Substituting $\mathbf{h}_k = \mathbf{g}_k \mathbf{\Psi}_f \mathbf{H}_k$ in (7), the SINR at the k-th user is written as

$$S_k = \frac{|\mathbf{h}_k^H \mathbf{w}_k|^2}{\sum\limits_{i\neq k} |\mathbf{h}_k^H \mathbf{w}_i|^2 + \mathbf{h}_k^H \mathbf{R}_r \mathbf{h}_k + \sigma_k^2} \tag{8}$$

D. Sensing SNR

The echo received at the BS utilizing the multi-sector RIS from the target is given by

$$\mathbf{y}_b = (\mathbf{g}_s \mathbf{\Psi}_t \mathbf{H}_k)^H (\mathbf{g}_s \mathbf{\Psi}_t \mathbf{H}_k) \left(\sum_{k=1}^{K} \mathbf{w}_k x_k + \mathbf{x}_t\right) + \mathbf{n}_b \tag{9}$$

where $\mathbf{n}_b \sim \mathcal{CN}(0, \sigma_b^2 \mathbf{I}_{M_t})$ is the AWGN at the BS. Substituting $\mathbf{g}_b = \mathbf{g}_s \mathbf{\Psi}_t \mathbf{H}_k$. Using a number of mathematical manipulations, the sensing SNR [22] may be expressed as

$$S_s = \| \mathbf{g}_b \|^2 \left(\sum_{k=1}^{K} |\mathbf{w}_k^H \mathbf{g}_b|^2 + \mathbf{g}_b \mathbf{R}_r \mathbf{g}_b^H\right) / \sigma_b^2. \tag{10}$$

III. Performance Analysis

In this section, we will start by evaluating the outage probability for the conventional STAR RIS and then later convert the composite channel to the proposed non-diagonal multi-sector RIS using order statistics. Since the RIS is partitioned into multiple sectors, users positioned closest to a given sector will experience an amplified signal from that sector. Consequently, the phase shift matrix will be transformed into an ordered matrix to optimize these gains.

A. OP of blocked user

OP is the probability that the SINR at the k-th user is below the SNR threshold level, denoted as

$$\mathcal{P}_{out}^k = \Pr\{S_k < S_{th_k}\} \tag{11}$$

where $S_{th_k} = 2^{R_{th_k}} - 1$ with R_{th_k} being the threshold rates of k-th user. For calculating the OP of the k-th user, the transmit beamforming vector $\mathbf{w}_k$ is obtained by the maximum ratio transmission (MRT) technique. It is given by $\mathbf{w}_k = \frac{\mathbf{h}_k^H}{\|\mathbf{h}_k^H\|}$. From (8) and (11), the OP can be rewritten as:

$$\mathcal{P}_{out}^k = \Pr\left\{ \| \mathbf{h}_k^H \|^2 < \frac{S_{th_k}(1+\rho_b \mathcal{I})}{\rho_b - \rho_r S_{th_k}} \right\} \tag{12}$$

where $\rho_b = \frac{P_b}{\sigma_k^2}$, and $\rho_r = \frac{P_r}{\sigma_k^2}$ are the transmit SNR for the communication and sensing signal. P_b and P_r are the power allocated to the message and sensing signal. $\mathcal{I} = \sum_{i\in\mathcal{K}, i\neq k} |\mathbf{h}_k^H \mathbf{w}_i|^2$ denotes the inter-user interference. For the conventional multi-sector RIS the norm of the composite channel is given by $\| \mathbf{h}_k \|^2 = \left(\sum_{r=1}^{R} h_{r,1} g_{k,r} \right)^2$, where $h_{r,1}$ and $g_{k,r}$ represents the individual elements of $\mathbf{H}_k$ and $\mathbf{g}_k$, respectively. With $|\mathbf{H}_k|$ and $|\mathbf{g}_k|$ being i.i.d. distributed, as given in [23], the multiplication of two random variables having Nakagami-m distribution results in the probability distribution function (PDF) that is represented as

$$f_{X_d}(x) = \frac{4\left(m_i m_x\right)^{\frac{m_i+m_x}{2}}}{\Gamma(m_i)\Gamma(m_x)} x^{m_i+m_x-1} I_{m_i-m_x}\left(2\sqrt{m_i m_l}x\right), \tag{13}$$

where $X_d = \|\mathbf{h}_k\|^2$, $m_i = \min\{m_1, m_2\}$, $m_x = \max\{m_1, m_2\}$, $I_{m_i-m_x}(\cdot)$ represents the modified Bessel function of the second kind and subscript X_d represents the PDF for diagonal STAR RIS. Due to the complexity in calculating $I_{m_i-m_x}(\cdot)$ in (13), we employ the Laplace transform (LT) of X_d, given as:

$$\mathcal{L}_{X_d}(s) = \mathbb{E}\left(e^{-s\|h_k\|^2}\right) = \frac{4\left(m_i m_x\right)}{\Gamma(m_i)\Gamma(m_x)} \times \int_0^\infty x^{m_i+m_x-1} e^{-sx} I_{t_s-t_l}\left(2\sqrt{m_i m_x}x\right) dx. \tag{14}$$

Using [24, eq. (6.621.3)], (14) can be reformulated as

$$\mathcal{L}_{X_d}(s) = m\left(s + 2\sqrt{m_i m_x}\right)^{-2m_i} \times F\left(2m_i, m_i - m_x + \frac{1}{2}; m_i + m_x + \frac{1}{2}; \frac{s - 2\sqrt{m_i m_x}}{s + 2\sqrt{m_i m_x}}\right), \tag{15}$$

where $m = \frac{\sqrt{\pi} 4^{m_i - m_x + 1} (m_i m_x)^{m_i} \Gamma(2m_i)\Gamma(2m_x - 2m_i)}{\Gamma(m_i \Gamma(m_x)\Gamma(m_i + m_x + 0.5)}$, and $F(\cdot,\cdot;\cdot;\cdot)$ represents hypergeometric series. Then, upon assuming $m_1 \neq m_2$ and $s \to \infty$, the LT is approximated as

$$\mathcal{L}_{X_d}(s) \approx m\left(s + 2\sqrt{m_i m_x}\right)^{-2m_i}. \tag{16}$$

Considering that the reflected links as i.i.d., the cumulative channel gain is computed as

$$\mathcal{L}_{X_d}(s) \approx m^R \left(s + 2\sqrt{m_i m_x}\right)^{-2m_i R}. \tag{17}$$

Utilizing the inverse LT in (17), the PDF is calculated as

$$f_{X_d}(x) = \frac{m^R}{2m_i R} x^{2m_i R - 1} e^{-2\sqrt{m_i m_x}x}, \tag{18}$$

The cumulative density function (CDF) of the composite channel is expressed as

$$F_{X_d}(x) = \frac{m^R \left(4 m_i m_x\right)^{-m_i R}}{\Gamma(2m_i R)} \gamma\left(2m_i R, 2\sqrt{m_i m_x}x\right). \tag{19}$$

The channel gain for the proposed non-diagonal multi-sector RIS is organized in ascending order and can be articulated through order statistics [25] as

$$F_{X_{nd}}(x) = \sum_{j=1}^{R} \binom{R}{j} [F_{X_d}(x)]^j [1 - F_{X_d}(x)]^{R-j} \tag{20}$$

where $\binom{R}{j} = \frac{R!}{j!(R-j)!}$, and $F_{X_{nd}}(x)$ represents the CDF. Using (12) and (19), the OP for UE$_k$ under composite fading in the multi-sector RIS setup can be expressed as

$$\begin{aligned} P_{out}^k = & \sum_{j=1}^{R} \binom{R}{j} \left[\frac{m^R \left(4 m_i m_x\right)^{-m_i R}}{\Gamma(2m_i R)}\right]^j \\ & \times \left[\gamma\left(2m_i R, 2\sqrt{m_i m_x} \frac{S_{th_k}(1+\rho_b \mathcal{I})}{\rho_b - \rho_r S_{th_k}}\right)\right]^j \\ & \times \left[1 - \frac{m^R \left(4 m_i m_x\right)^{-m_i R}}{\Gamma(2m_i R)} \right. \\ & \left. \times \gamma\left(2m_i R, 2\sqrt{m_i m_x} \frac{S_{th_k}(1+\rho_b \mathcal{I})}{\rho_b - \rho_r S_{th_k}}\right)\right]^{R-j}. \end{aligned} \tag{21}$$

B. Sensing Rate

From an informational standpoint, the evaluation of ISAC system performance depends on the key metric known as the sensing rate (SR). This metric gauges the information-theoretic boundaries governing the retrieval of environmental information. Without the loss of generality, the sensing rate is written as

$$\begin{aligned} R_s &= \frac{1}{\log(2)} \mathbb{E}\left[\log(1 + S_s)\right] \\ &= \frac{1}{\log(2)} \mathbb{E}\left[\log\left(1 + \frac{\| \mathbf{g}_b \|^2}{\sigma_b^2} \left(\sum_{k=1}^{K} |\mathbf{w}_k^H \mathbf{g}_b|^2 + \mathbf{g}_b \mathbf{R}_r \mathbf{g}_b^H\right)\right)\right]. \end{aligned} \tag{22}$$

Considering the transmit beamforming vector be designed using the maximum ratio transmission (MRT) technique and $\mathcal{I}_s = \sum_{i\in\mathcal{K}, i\neq k} |\mathbf{w}_i^H \mathbf{g}_b|^2$. The distribution of $\|\mathbf{g}_b\|^2$ is considered to be similar to $\|\mathbf{h}_k\|^2$. The sensing rate is expressed as

$$\begin{aligned} R_s = & \int_0^\infty \frac{1}{\log(2)} \log\left(1 + x(\rho_b x + \rho_s x + \rho_b \mathcal{I}_s)\right) \sum_{j=1}^{R} \binom{R}{j} f_{X_d}(x) \\ & \times \left[F_{X_d}(x)\right]^{j-1} \left[1 - F_{X_d}(x)\right]^{R-j-1} \left(j - R F_{X_d}(x)\right) dx. \end{aligned} \tag{23}$$

C. System Throughput

The system throughput is evaluated by computing the OP at a specified rate, represented as R_i. The throughput of the proposed multi-sector RIS MISO network is described as

$$T_{sys} = (1 - P_{out}^k) R_{th_k}, \tag{24}$$

where P_{out}^k is the outage probability at the UE$_k$ given in (21).

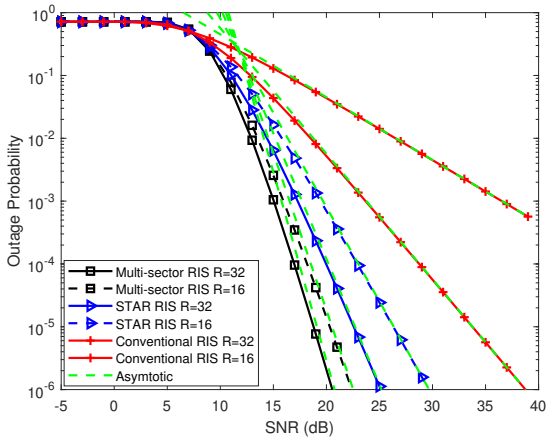

Fig. 2: Outage probability comparison between the proposed multi-sector RIS, the STAR RIS, and the conventional RIS.

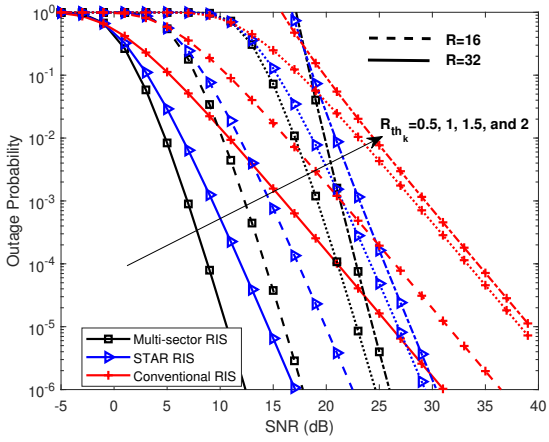

Fig. 3: Outage probability of users as a function of transmit SNR for various threshold rate values.

IV. Results and Discussions

The section discusses results obtained from analyzing the proposed multi-sector RIS system. The analysis is verified through Monte Carlo simulations. In which, we assume a BS to be equipped with 4 antennas, communicating with $K = 4$ users while performing target detection using the proposed multi-sector RIS, which consists of R elements. The transmit power is $P_b = 10$W, and the noise power is $\sigma^2 = -80$ dBm. The interference power is assumed to be $\mathcal{I} = \mathcal{I}_s = -50$dBm.

A. Outage Probability

Fig. 2 plots the OP of the proposed multi-sector RIS with the SNR for $m_1 = 2$, $m_2 = 1$. The number of multi-sector RIS elements is also varied from $R = 16$ to $R = 32$. The target rates for the UE$_k$ is $R_{th_k} = 1$ bits per channel use (BPCU). (21) is used to plot the outage probability of UE$_k$. The curves generated from numerical simulations closely match the expressions derived in the previous sections. Increasing R improves channel gain and outage probability. The red, black, blue, and magenta curves indicate the OP as the R increases from $R = 16$, and 32, respectively. This indicates that increasing R reduces the OP. Furthermore, the solid lines represent the proposed multi-sector RIS, and the dashes denote the conventional STAR RIS. It is evident that the proposed system showed improved performance than the conventional STAR RIS. The performance gain is obtained because the channel gain of the multi-sector RIS is obtained after sorting the channels in ascending order, which results in a higher overall gain than that of the conventional STAR RIS. Fig. 3 illustrates the OP of multi-sector RIS networks by considering different target rates. The red, black, blue, and magenta curves indicate the outage probability as the target rate increases from $R_{th_k} = 0.5, 1, 1.5$, and 2 BPCU, respectively. R is set to 16 to obtain the plot. An important observation is that higher target rates in multi-sector RIS networks result in increased OP. This is due to the relationship between threshold rates and the required SNRs.

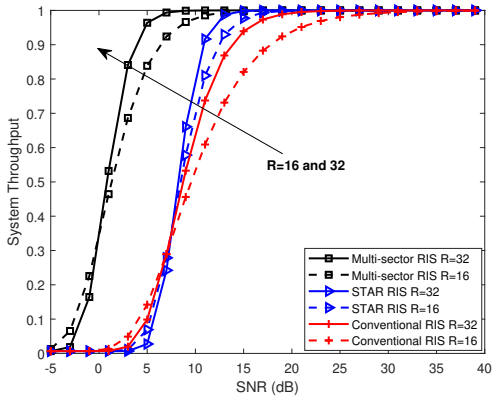

Fig. 4: System throughput versus transmit SNR.

B. System Throughput

The system throughput for the designed multi-sector RIS network in the downlink is illustrated against the transmit SNR in Fig. 4, with $R_{th_k} = 1$ bits per channel use (BPCU). The curves are derived from equation (24). The plot demonstrates that the throughput of the multi-sector RIS configuration consistently outperforms the conventional STAR RIS setup across all SNR levels, mainly due to the influence of OP on throughput performance. As the number of reflective elements grows, the proposed structure achieves higher throughput, attributed to improved outage characteristics for user UE$_k$. Additionally, an increase in RIS elements contributes to enhanced spectral efficiency.

C. Sensing Rate

Fig. 5 plots the sensing rate of the proposed system versus the SNR with setting to be $m_1 = 2$, $m_2 = 1$, for different numbers of RIS sector elements R. (23) is used to plot the sensing rate. The figure reveals that the sensing rate of

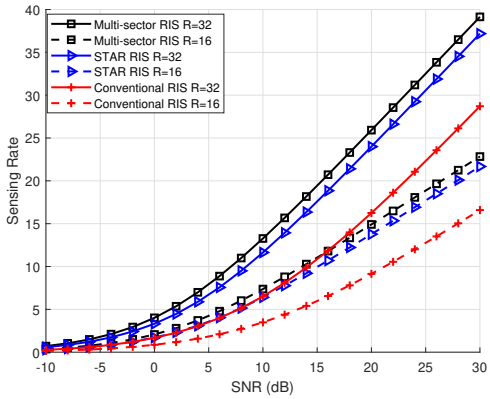

Fig. 5: Sensing Rate comparison between multi-sector, STAR and conventional RIS.

the proposed multi-sector RIS is greater than conventional STAR RIS. This enhancement is attributed to the multi-sector design, which allows users nearest to each sector to benefit from focused, sector-specific signal amplification. Furthermore, increasing R improves the system's sensing rate because a higher R enables greater flexibility in the ordered phase shift matrix, further boosting the sensing rate.

V. Conclusion

In conclusion, this paper presents a novel framework for multi-sector RIS-assisted MISO networks with ISAC for 6G applications. By partitioning the RIS into independently controlled sectors, each capable of dynamic phase-shift adjustments and sector-specific transmission or reflection, the proposed system effectively targets distributed users while simultaneously supporting target detection through ISAC. The derived closed-form outage probability expressions validate the reliability of the nearest-sector selection strategy, particularly under blocked direct link conditions between the BS and users. Additionally, sensing performance is enhanced by calculating the sensing rate within each sector, revealing that an increased number of RIS elements significantly boosts target detection capabilities. Comparative analyses demonstrate that this multi-sector multi-sector RIS architecture outperforms conventional RIS and STAR RIS, substantially improving communication and sensing metrics. This framework highlights the potential of sectorized RIS to drive advanced applications in next-generation IoT networks.

References

[1] D. C. Nguyen, M. Ding, P. N. Pathirana, A. Seneviratne, J. Li, D. Niyato, O. Dobre, and H. V. Poor, "6G internet of things: A comprehensive survey," *IEEE Internet Things J.*, vol. 9, no. 1, pp. 359–383, 2021.

[2] Y. Xu, G. Gui, H. Gacanin, and F. Adachi, "A survey on resource allocation for 5G heterogeneous networks: Current research, future trends, and challenges," *IEEE Commun. Surveys Tuts.*, vol. 23, no. 2, pp. 668–695, 2021.

[3] C. Xu, B. Clerckx, S. Chen, Y. Mao, and J. Zhang, "Rate-splitting multiple access for multi-antenna joint radar and communications," *IEEE J. Sel. Topics Sig. Process.*, vol. 15, no. 6, pp. 1332–1347, 2021.

[4] J. A. Zhang *et al.*, "An overview of signal processing techniques for joint communication and radar sensing," *IEEE J. Sel. Topics Signal Process.*, vol. 15, no. 6, pp. 1295–1315, 2021.

[5] F. Liu *et al.*, "Integrated sensing and communications: Toward dual-functional wireless networks for 6G and beyond," *IEEE J. Sel. Areas Commun.*, vol. 40, no. 6, pp. 1728–1767, 2022.

[6] S. Hu, F. Rusek, and O. Edfors, "Beyond massive MIMO: The potential of data transmission with large intelligent surfaces," *IEEE Trans. Signal Process.*, vol. 66, no. 10, pp. 2746–2758, 2018.

[7] L. Dai, B. Wang, M. Wang, X. Yang, J. Tan, S. Bi, S. Xu, F. Yang, Z. Chen, M. Di Renzo *et al.*, "Reconfigurable intelligent surface-based wireless communications: Antenna design, prototyping, and experimental results," *IEEE Access*, vol. 8, pp. 45 913–45 923, 2020.

[8] C. Pan, H. Ren, K. Wang, J. F. Kolb, M. Elkashlan, M. Chen, M. Di Renzo, Y. Hao, J. Wang, A. L. Swindlehurst *et al.*, "Reconfigurable intelligent surfaces for 6G systems: Principles, applications, and research directions," *IEEE Commun. Mag.*, vol. 59, no. 6, pp. 14–20, 2021.

[9] A. S. Parihar, K. Singh, V. Bhatia, C.-P. Li, and T. Q. Duong, "Performance analysis of NOMA-enabled active RIS-aided MIMO heterogeneous IoT networks with integrated sensing and communication," *IEEE Internet Things J.*, vol. 11, no. 17, pp. 28 137–28 152, 2024.

[10] K. Singh, F. Karim, S. K. Singh, P. K. Sharma, S. Mumtaz, and M. F. Flanagan, "Performance analysis of RIS-assisted full-duplex communications with infinite and finite blocklength codes," *IEEE Trans. Commun.*, vol. 71, no. 7, pp. 4262–4282, 2023.

[11] T. Van Chien, A. K. Papazafeiropoulos, L. T. Tu, R. Chopra, S. Chatzinotas, and B. Ottersten, "Outage probability analysis of irs-assisted systems under spatially correlated channels," *IEEE Wireless Commun. Lett.*, vol. 10, no. 8, pp. 1815–1819, 2021.

[12] H. Ibrahim, H. Tabassum, and U. T. Nguyen, "Exact coverage analysis of intelligent reflecting surfaces with Nakagami-m channels," *IEEE Trans. Veh. Technol.*, vol. 70, no. 1, pp. 1072–1076, 2021.

[13] A. M. Salhab and M. H. Samuh, "Accurate performance analysis of reconfigurable intelligent surfaces over Rician fading channels," *IEEE Wireless Commun. Lett.*, vol. 10, no. 5, pp. 1051–1055, 2021.

[14] R. Deshpande, M. V. Katwe, K. Singh, and Z. Ding, "Resource allocation design for spectral-efficient URLLC using RIS-aided FD-NOMA system," *IEEE Wireless Commun. Lett.*, vol. 12, no. 7, pp. 1209–1213, 2023.

[15] J. Xu, J. Zuo, J. T. Zhou, and Y. Liu, "Active simultaneously transmitting and reflecting (STAR)-RISs: Modeling and analysis," *IEEE Commun. Lett.*, vol. 27, no. 9, pp. 2466–2470, 2023.

[16] Q. Gao, Y. Liu, X. Mu, M. Jia, D. Li, and L. Hanzo, "Joint location and beamforming design for STAR-RIS assisted NOMA systems," *IEEE Trans. Commun.*, vol. 71, no. 4, pp. 2532–2546, 2023.

[17] Q. Li *et al.*, "Reconfigurable intelligent surfaces relying on non-diagonal phase shift matrices," *IEEE Trans. Veh. Technol.*, vol. 71, no. 6, pp. 6367–6383, 2022.

[18] Y. Pan, Z. Qin, J.-B. Wang, Y. Chen, H. Yu, and A. Tang, "Joint deployment and beamforming design for STAR-RIS aided communication," *IEEE Commun. Lett.*, vol. 27, no. 11, pp. 3083–3087, 2023.

[19] R. Liu, M. Li, Y. Liu, Q. Wu, and Q. Liu, "Joint transmit waveform and passive beamforming design for RIS-aided DFRC systems," *IEEE J. Sel. Topics Sig. Process.*, vol. 16, no. 5, pp. 995–1010, 2022.

[20] Q. Tao, J. Wang, and C. Zhong, "Performance analysis of intelligent reflecting surface aided communication systems," *IEEE Commun. Lett.*, vol. 24, no. 11, pp. 2464–2468, 2020.

[21] H. Hua, J. Xu, and T. X. Han, "Optimal transmit beamforming for integrated sensing and communication," *IEEE Trans. Veh. Technol.*, 2023.

[22] D. Li, Z. Yang, N. Zhao, Z. Wu, and T. Q. S. Quek, "Noma aided secure transmission for irs-isac," *IEEE Transactions on Wireless Communications*, vol. 23, no. 9, pp. 10 911–10 925, 2024.

[23] N. Bhargav, C. R. N. da Silva, Y. J. Chun, É. J. Leonardo, S. L. Cotton, and M. D. Yacoub, "On the product of two $\kappa-\mu$ random variables and its application to double and composite fading channels," *IEEE Trans. Wireless Commun.*, vol. 17, no. 4, pp. 2457–2470, 2018.

[24] I. S. Gradshteyn and I. M. Ryzhik, *Table of Integrals, Series, and Products*. 6th ed. New York, NY, USA: Academic Press, 2000.

[25] K. Subrahmaniam, "On some applications of Mellin transforms to statistics: Dependent random variables," *SIAM J. Appl. Mathematics*, vol. 19, no. 4, pp. 658–662, 1970.